PHYSICAL REVIEW B VOLUME 44, NUMBER 10 1 SEPTEMBER 1991-II

Luminescence thermal quenching of Cr^{3+} in zirconium-barium-based fluoride glasses investigated by time-resolved laser spectroscopy

R. Balda, J. Fernández, and M. A. Illarramendi
Departamento de Física Aplicada I, Escuela Técnica Superior de Ingenieros Industriales y de Telecomunicación, Universidad del País Vasco, Alameda Urquijo s/n 48013 Bilbao Spain

M. A. Arriandiaga
Departamento de Física Aplicada II, Facultad de Ciencias, Universidad del País Vasco, Apartado 644, Bilbao, Spain

J. L. Adam and J. Lucas
Laboratoire de Chimie Minérale D, Université de Rennes, Campus de Beaulieu, Avenue du Général Leclerc, 35042 Rennes CEDEX, France

(Received 12 February 1991)

The optical properties of trivalent chromium ions in zirconium-barium-lanthanum fluoride glasses [$62ZrF_4$-$30BaF_2$-$8LaF_3$, $57ZrF_4$-$34BaF_2$-$5LaF_3$-$4AlF_3$, and 58 ZrF_4-$18BaF_2$-$5.5LaF_3$-$3AlF_3$-$15NaF$] have been investigated by using steady-state and time-resolved luminescence techniques. The thermal quenching of the broadband emission is discussed in terms of the quantum-mechanical single-configurational-coordinate model using the Struck-Fonger method, and good agreement with the experimental results is obtained. The quantum efficiencies for the three glasses are low in accordance with the strong thermal quenching of the luminescence, and the influence of the host material on their values can be well related with the parameters of the quantum-mechanical single-configurational-coordinate model. In order to correlate glass-matrix composition with emission spectral properties, detailed time-resolved measurements have been performed. The results obtained provide evidence for the assumption of two main statistical site distributions for Cr^{3+} in these glasses.

I. INTRODUCTION

In the last few years an increasing interest has arisen in the study of heavy-metal fluoride glasses (HMFG's) related to passive and active optical applications including multispectral optical components, optical fibers, fiber lasers, and amplifiers.[1-5] The optical properties of rare earth and transition metal ions in HMFG's have been intensively investigated by many authors.[6-12] The spectroscopic properties of Cr^{3+} in glasses have attracted much attention over the past few years because of applications to lasers[13] and solar concentrators.[14] It is specially interesting to consider Cr^{3+} ions in hosts with a weak crystal-field environment because a large vibronically broadened ${}^4T_2 \rightarrow {}^4A_2$ emission occurs, and lasers with a wide tuning range may be constructed. However, there have been only a few studies on the optical properties of Cr^{3+} in fluoride glasses because of the low efficiency and thermal quenching of the emission. The low efficiency for Cr^{3+} emission in glasses is attributed to the high probability for nonradiative transitions.[15] More recently, it has been explained in terms of the loose nature of the glass structure and the importance of local bonding requirements in determining the environment of the Cr^{3+} ions in the glass.[16,17]

In a recent work,[18] the authors investigated the optical properties of the same ion in a HMF matrix of composition $30BaF_2$-$18InF_3$-$12GaF_3$-$20ZnF_2$-$10YF_3$-$10ThF_4$ (BIGaZYT). In this study the thermal quenching of the luminescence was discussed in terms of the quantum-mechanical single-configurational-coordinate (QMSCC) model,[19] and a quite good agreement with the experimental results was found. The spectroscopic data pointed out the existence of two main site distributions for the Cr^{3+} ions. Evidence for this assumption was also found in a preliminary characterization of the optical properties of this ion in $57ZrF_4$-$34BaF_2$-$5LaF_3$-$4AlF_3$ (ZBLA) glass.[20]

The aim of this work is to give a deeper understanding of the optical properties of Cr^{3+} in zirconium-barium-fluoride glasses (ZBL, ZBLA, and ZBLAN) and to study the influence of the glass composition on its spectral and temperature behavior. It will be shown that the QMSCC model (no linear coupling) allows a qualitative prediction of the temperature dependence of the nonradiative probabilities of the ${}^4T_2 \rightarrow {}^4A_2$ emission for the three samples. The parameter values obtained from this model can be correlated with the influence of the host material on the quantum efficiency of Cr^{3+}.

In order to establish a further correlation between glass-matrix composition and emission spectral properties, detailed time-resolved photoluminescence measurements have been performed for the three glasses. The results obtained provide evidence for the assumption of two main statistical site distributions for Cr^{3+} ions in these glasses.

II. EXPERIMENTAL TECHNIQUES

The fluoride glasses used in this study were prepared at the Mineral Chemistry Laboratory of the Rennes University (France).

Samples were obtained with the molar composition $62ZrF_4$-$30BaF_2$-$8LaF_3$ (ZBL), $57ZrF_4$-$34BaF_2$-$5LaF_3$-$4AlF_3$ (ZBLA), and $58ZrF_4$-$18BaF_2$-$5.5LaF_3$-$3AlF_3$-$15NaF$ (ZBLAN). The experimental method for preparing the glass has been well described in the literature.[5,21] Briefly, after fluorination of the starting oxide materials at 350 °C, the mixture is melted under a controlled atmosphere. Then the melt is poured into a brass mold and annealed at a temperature slightly above the glass temperature T_g. Finally, the samples are cut and polished for optical measurements. The samples used in this work were doped with 0.5 at. % Cr^{3+}.

The sample temperature was varied between 4.2 and 300 K with a continuous flow cryostat. Conventional absorption spectra were performed with a CARY 17 spectrophotometer. The emission measurements were made using the 633-nm emission line of a 15-mW He-Ne laser and the 476- and 514-nm emission lines of an argon laser as exciting light. The fluorescence was analyzed with a 0.22-m SPEX monochromator, and the signal was detected by a Hamamatsu R7102 extended ir photomultiplier and finally amplified by a standard lockin technique. The system response was calibrated with a standard tungsten-halogen lamp to correct the emission spectra.

Lifetime measurements were performed with a tunable dye laser (1-ns pulse width). In order to describe the evolution of fluorescence, time-resolved spectroscopy has been used. The emission measurements were obtained by exciting the sample with a tunable dye laser and detecting the emission with a Hamamatsu R7102 photomultiplier. The spectra were processed by a EGG-PAR boxcar integrator.

III. EXPERIMENTAL RESULTS

A. Absorption and emission spectra

In spite of the expected sensitivity to variations of the local Cr^{3+} environments, the main features of the absorption spectra of Cr^{3+} are only slightly influenced by the nature of the glass hosts.[22] This prominent role played by the bonding in the Cr^{3+} site can be understood by assuming that, on the average, the chromium ions occupy sites that have nearly octahedral symmetry due to the strong ligand field stabilization energy of Cr^{3+} in a sixfold coordination. It is well known that parity-forbidden *d-d* excitations in transition-metal ions can be partially allowed if cubic symmetry is slightly distorted by the presence of a weak low-symmetry field of odd parity or if it is instantaneously distorted by the presence of odd-parity molecular vibrations. In the latter case, it can be proved[23] that absorption oscillator strength values are independent of the form of the excited-state potential-energy curve even if the excited state involves a change in geometry, force constant, or anharmonicity with respect to the odd-parity nuclear coordinates. Therefore the absorption and emission spectra are usually interpreted by the Tanabe-Sugano diagram for d^3 systems with octahedral coordination, at least as far as the energy levels are concerned.[15,24,25]

Figure 1 shows the emission and absorption spectra of Cr^{3+} in ZBL, ZBLA, and ZBLAN obtained at liquid-nitrogen temperature (LNT). The absorption spectra are characterized by two broad spin-allowed bands, which can be identified as the vibronically broadened transitions ${}^4T_2 \leftarrow {}^4A_2$, ${}^4T_1(t_2^2e) \leftarrow {}^4A_2$ in order of increasing energy. The low-energy band shows a fine structure due to the spin-forbidden ${}^2E \leftarrow {}^4A_2$ and ${}^2T_1 \leftarrow {}^4A_2$ transitions. The assignment of this structure has been made following the Fano antiresonance interpretation.[26,27] Not shown in this figure, a higher-energy transition ${}^4T_1(t_2e^2) \leftarrow {}^4A_2$ is also found in ZBL and ZBLAN.

In agreement with the predictions of the d^3 Tanabe-Sugano diagram in octahedral symmetry, the energies of ${}^2E \leftarrow {}^4A_2$ ($\approx 15\,208$ cm^{-1}) and ${}^2T_1$ ($\approx 15\,966$ cm^{-1}) do not show any appreciable change with the host lattice, whereas the transition energies to ${}^4T_2$ and ${}^4T_1$ states do vary somewhat due to differences of the crystal field of the different hosts. The ${}^4T_1(t_2^2e) \leftarrow {}^4A_2$ transitions are centered around 22 222 cm^{-1} (ZBL), 22 436 cm^{-1} (ZBLA), and 22 310 cm^{-1} (ZBLAN), whereas the ${}^4T_2 \leftarrow {}^4A_2$ transitions occur around 15 176 cm^{-1} (ZBL), 15 310 cm^{-1} (ZBLA), and 15 263 cm^{-1} (ZBLAN).

The emission measurements were made under excita-

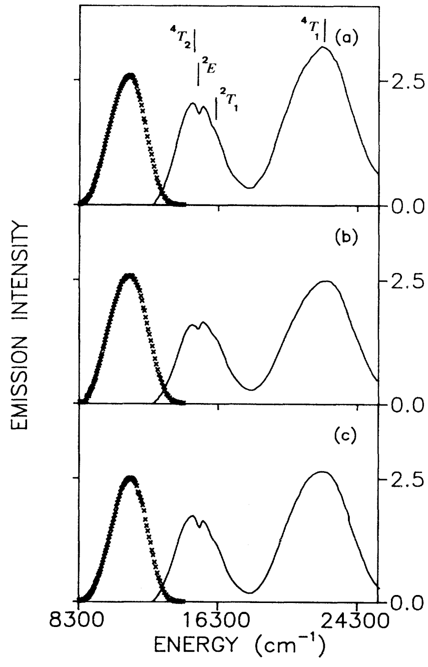

FIG. 1. Absorption (solid line) and emission (×) spectra at LNT. (a) ZBL:Cr^{3+}. (b) ZBLA:Cr^{3+}. (c) ZBLAN:Cr^{3+}. The emission spectra were corrected for instrumental response and were excited with the 633-nm line of a He-Ne laser.

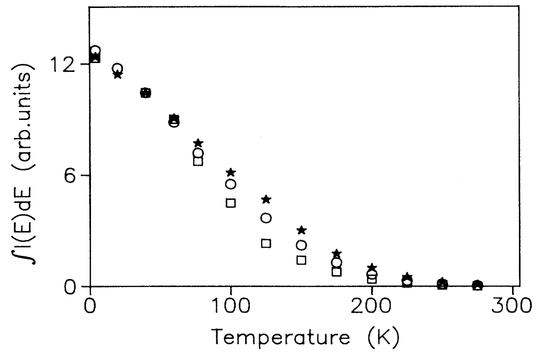

FIG. 2. Integrated emission intensities $\int I(E)dE$ as a function of temperature for the three samples: (□) ZBL, (○) ZBLA, and (★) ZBLAN.

tion in the ${}^4T_2 \leftarrow {}^4A_2$ absorption band using the 633 nm line of a He-Ne laser. Additional measurements under excitation in the ${}^4T_1(t_2^2e) \leftarrow {}^4A_2$ absorption band will be also shown in Sec. IV C. The emission in these glasses is characterized by a broad and structureless band that corresponds to the ${}^4T_2 \rightarrow {}^4A_2$ transition. For a 633-nm excitation wavelength, as can be seen in Fig. 1, the peak position; 11 031 cm^{-1} (ZBL), 11 124 cm^{-1} (ZBLA), and 11 178 cm^{-1} (ZBLAN), and the bandwidth, 935 cm^{-1} (ZBL), 981 cm^{-1} (ZBLA), and 932 cm^{-1} (ZBLAN), are similar for the three samples. In all cases a large Stokes shift ($\approx$4000 cm^{-1}) is observed, indicating that a considerable change occurs in the ionic arrangement around Cr^{3+} in the excited state.[17] In Fig. 2 a plot of the integrated emission intensity as a function of temperature for the three samples is presented, and it shows that the intensity decreases as temperature increases, which is due to increasing nonradiative processes.

Table I contains a summary of LNT spectroscopic data of Cr^{3+} in these glasses. The crystal-field parameters Dq and B were calculated by using the Tanabe-Sugano matrix elements.[28] The ${}^4T_2$ emission peak position was used to determine a value of Dq/B for the relaxed excited state (RES) from the formula

$$\left[\frac{Dq}{B}\right]_{\mathrm{RES}} = \frac{E({}^4T_2 \rightarrow {}^4A_2)}{10B} , \tag{1}$$

where $E({}^4T_2 \rightarrow {}^4A_2)$ is the energy of the peak position of the emission band, and the value of B is assumed to remain unchanged by the variation of the Cr-F distance.

The oscillator strengths, in absorption, have been estimated by using standard relations.[29] To estimate the radiative lifetime we use the approximate relation[29]

$$f_{\mathrm{em}}\tau_R = 1.51\times 10^4 \frac{9}{n(n^2+2)^2}\lambda^2 , \tag{2}$$

where n is the refractive index, λ is the emission peak in meter units, and f_{em} is the oscillator strength, which is related to the one in absorption f_{abs} by

$$\frac{f_{\mathrm{em}}}{f_{\mathrm{abs}}} = \frac{\omega_{\mathrm{em}}}{\omega_{\mathrm{abs}}} = \frac{\lambda_{\mathrm{abs}}}{\lambda_{\mathrm{em}}} , \tag{3}$$

where λ_{abs}, and λ_{em} are the peak positions of absorption and emission ${}^4A_2 \leftrightarrow {}^4T_2$ transition, respectively. A more accurate relation can be found in the McCumber theory,[30] but such refinement does not seem to be justified for the HMF systems studied.

TABLE I. LNT spectroscopic data of the three doped glasses. Dq/B is the octahedral crystal field, f_{abs} is the oscillator strength of ${}^4A_2 \rightarrow {}^4T_2$, τ_R is the radiative lifetime, $(Dq/B)_{\mathrm{RES}}$ is the crystal field for the relaxed excited state, ΔE_s is the Stokes shift, and τ_{exp} is the average lifetime monitored at the emission peak.

	ZBL	ZBLA	ZBLAN
Dq/B	2	2.01	1.96
f_{abs}	1.85×10^{-5}	1.61×10^{-5}	1.66×10^{-5}
τ_R (μs)	293.38	334.3	321.75
$(Dq/B)_{\mathrm{RES}}$	1.46	1.47	1.45
ΔE_s (cm^{-1})	4121	4186	3960
τ_{exp} (μs)	90.5	90	99

B. Emission lifetime results

The decay kinetics of the broad infrared emission of the three samples were studied as a function of temperature, emission, and excitation wavelength.

The observed decays measured along the broad emis-

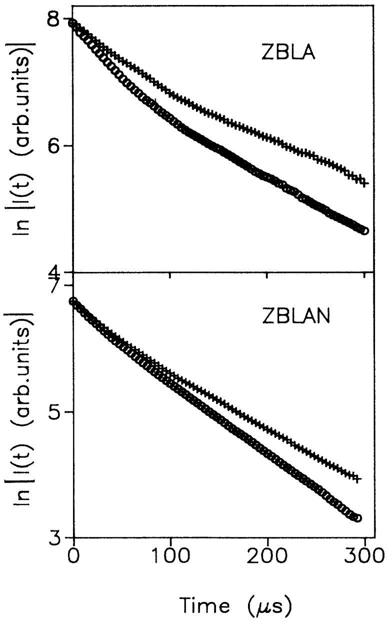

FIG. 3. Logarithmic plot of the decays monitored at 760 nm (+) and 1050 nm (○) for ZBLA:Cr^{3+}, and at 790 (+) and 1000 (○) for ZBLAN:Cr^{3+}. Measurements were performed at 77 K, for an excitation wavelength of 655 nm.

TABLE II. Long-lived (τ_l), and short-lived (τ_s) components of the experimental decays at different emission wavelengths, obtained by a least-squares fit for ZBLA:Cr^{3+}, and ZBLAN:Cr^{3+} samples.

Glass / Emission wavelength (nm)	ZBLA 760	ZBLA 1050	ZBLAN 790	ZBLAN 1000
τ_l (μs)	158	117	152	135
τ_s (μs)	44	32	49	33

sion band, under pulsed laser excitation, at the center of the $^4T_2 \leftarrow {}^4A_2$ absorption band, can be described for the three samples, throughout the whole temperature range, by a double exponential function. This behavior persists even at lower concentrations ($\approx$0.05%); therefore, chromium-chromium interactions are not considered to be important in this analysis. Figure 3 shows, as an example, the logarithmic plot of the intensity decay at LNT for emission wavelengths at the blue and red sides of the emission band for ZBLA and ZBLAN samples. The short-lived and long-lived components of the experimental decays obtained by a least-squares fit are presented in Table II. These calculated values are only a qualitative indication of the biexponential character of the decays. For practical purposes we shall use the "average lifetime" defined by equation $\bar{\tau} = \int tI(t)dt / \int I(t)dt$ in the analysis that follows. It is worthwhile noticing that the calculated $\bar{\tau}$ are very close to the τ values obtained by fitting the experimental curves to a single exponential function (deviations $|\bar{\tau} - \tau|$ are less than 10%), indicating the weak biexponential character of the decays.

The fluorescence decays at different emission wavelengths along the $^4T_2 \rightarrow {}^4A_2$ emission band for the three samples are plotted in Fig. 4. In all cases the lifetime remains nearly constant on the high-energy wing, and then decreases linearly as the energy decreases throughout the $^4T_2 \rightarrow {}^4A_2$ emission band. As can be seen, the decays show a similar behavior in ZBL and ZBLA compounds, whereas in the ZBLAN case the wavelength slope is somewhat higher.

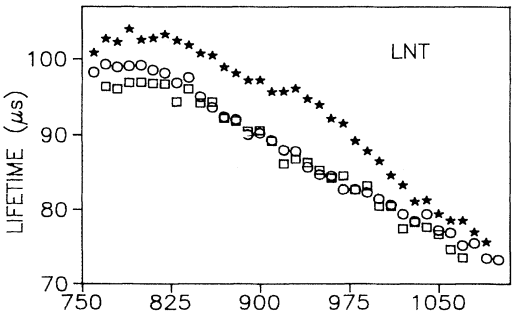

FIG. 4. LNT lifetimes at different emission wavelengths along the $^4T_2 \rightarrow {}^4A_2$ emission band for an excitation wavelength of 655 nm. The data correspond to the average lifetime: (□) ZBL:Cr^{3+}, (○) ZBLA:Cr^{3+}, and (★) ZBLAN:Cr^{3+}.

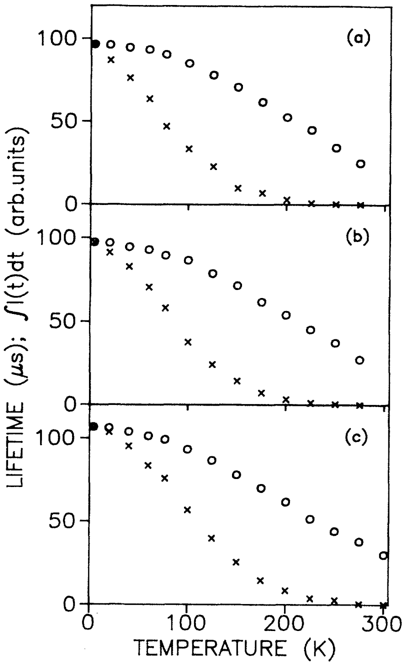

FIG. 5. Emission lifetimes (○) and integrated emission intensities (×) as a function of temperature for Cr^{3+} in the matrices (a) ZBL, (b) ZBLA, and (c) ZBLAN. Lifetimes were obtained by exciting at 655 nm, and collecting at the emission peaks.

The fluorescence decays at different excitation wavelengths were also measured. The decays obtained by collecting the fluorescence at the peak position of the emission band, under excitation on the $^4T_2 \leftarrow {}^4A_2$ absorption band, do not vary significantly between 620 and 670 nm, whereas they linearly decrease (about 10%) as excitation wavelength increases between 670 and 685 nm. The full range of the absorption band could not be completed due to dye limitations, and decays were too weak to be accurately measured above 685 nm.

Lifetime data, monitored at the peak position of the emission bands, and integrated emission intensities $\int I(t)dt$ as a function of temperature are shown in Fig. 5. It is apparent from this figure that the emission lifetimes and the integrated intensities display a similar qualitative behavior with temperature.

C. Time-resolved spectra

The variation of fluorescence lifetime with emission wavelength, and the double exponential character of the decays suggested the existence of some kind of site distribution for the Cr^{3+} ions. In order to obtain a more precise knowledge about this possibility, time-resolved emission and excitation spectra were performed.

Time-resolved emission spectra (TRS) were obtained at 77 K after exciting the samples with a tunable laser at the peak position of the low-energy absorption band. The evolution of the emission intensity at different time delays between 1 and 300 μs was investigated for the three samples. At shorter time delays the spectra present similar features to the steady-state (SS) emission spectra, but for increasing time delays they show a blue shift and a narrowing of the bandwidth. Figure 6 displays the first and second moments, calculated from the emission spectra, for ZBLA:Cr^{3+} and ZBLAN:Cr^{3+} as a function of time. As shown in this figure, the narrowing of the spectra and the peak shift do not exhibit a monotonic variation when time increases as was observed in other systems.[31] In this case the variation is more pronounced at the first 50 μs, corresponding this time with the values for the short-lived component of the decays. (See Table II.)

The LNT excitation spectra were performed by exciting the samples with a tunable dye laser and collecting the luminescence at three different wavelengths along the ${}^4T_2 \rightarrow {}^4A_2$ emission band, and at different time delays (1–300 μs). Figure 7 shows, as an example, the excitation spectra of the ${}^4T_2 \leftarrow {}^4A_2$ band for luminescence monitored at 760 nm (at the high-energy wing), and 900 nm (at the peak position of the emission band), at a time delay of 10 μs (gate width 50 ns). The excitation spectra are not corrected for the dye fluorescence. As can be seen, the high-energy spectrum is slightly blue shifted. No differences were observed between the spectrum obtained by collecting the luminescence at the low-energy wing of the emission band (1100 nm) and at the peak position (900 nm). A similar behavior was found in the three samples. It was difficult to analyze the evolution of the time-resolved excitation spectra because of the narrow spectral range of the excitation wavelengths (610–700 nm) provided by the DCM dye. Probably due to this limitation, no significant differences were observed at different time delays.

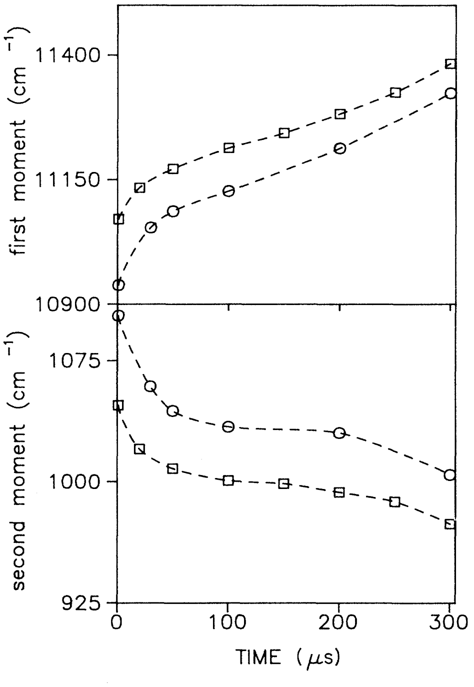

FIG. 6. Time dependence of first and second moments obtained from the corrected time-resolved emission spectra: (□) ZBLAN and (○) ZBLA. The time-resolved emission spectra were obtained by exciting at 655 nm with time delays between 1 and 300 μs, and gate widths between 20 ns, and 1 μs. The spectra were performed at 77 K. Dashed lines are only a guide for the eyes.

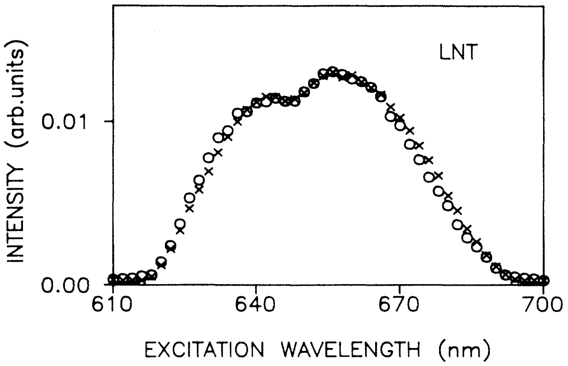

FIG. 7. LNT excitation spectra of the ${}^4T_2 \leftarrow {}^4A_2$ transition at a time delay of 10 μs (gate 50 ns) for luminescence monitored at 760 nm (○) and 900 mn (×). The spectra corresponds to ZBLAN:Cr^{3+} sample.

IV. DISCUSSION

A. Analysis of the emission spectra

The preceding spectroscopic data show that when Cr^{3+} is raised to the ${}^4T_2$ excited state, a large configurational relaxation occurs (RES) due to strong electron-phonon interactions. The spectroscopic features of the broad-band emission from the RES level can usually be described by a single-configurational-coordinate (SCC) model. The parameters of this model, in the linear coupling approximation, were calculated from the moment analysis of the emission bands. The quantitative analysis of luminescence spectra required a transformation from corrected intensities to line shapes $G(E)$.[32] The temperature dependence (4.2–300 K) of the second moment of the emission bands allows us to estimate the average "effective" frequency of the breathing mode and the average Huang-Rhys factor for the three samples. The obtained values were $\hbar\omega_0 = 518\ \mathrm{cm}^{-1}$ (ZBL), $\hbar\omega_0 = 500\ \mathrm{cm}^{-1}$ (ZBLA), and $\hbar\omega_0 = 566\ \mathrm{cm}^{-1}$ (ZBLAN), and $S = 3.3$ (ZBL), $S = 3.8$ (ZBLA), and $S = 2.7$ (ZBLAN). From the relation $h\nu_{0\mathrm{em}} = U_0 - S\hbar\omega_0$, the value for the electronic energy gap U_0 at 4.2 K for each sample was also obtained. The activation energy corresponding to the crossover point of the ground and excited-state-potential energies was calculated by using the relation

$$E_A = \frac{(U_0 - S\hbar\omega_0)^2}{4S\hbar\omega_0} \; . \tag{4}$$

Taking the above-mentioned S, $\hbar\omega_0$, and U_0 values, we found $E_A = 17\,849$ cm^{-1} (ZBL), 16 158 cm^{-1} (ZBLA), and 20 069 cm^{-1} (ZBLAN).

The fit of the emission line shape $G(E)$ predicted by the SCC model with linear coupling,[33] using the model parameters obtained, is quite poor, and the calculated Stokes shifts underestimate the experimental values.

B. Thermal quenching

The strong temperature dependence of the emission shown in Fig. 2 could be related either to energy transfer or to multiphonon transitions between electronic levels. Although the energy transfer is quite common in glassy materials because of the spectral overlap between absorption and emission bands, in our case this overlap shows a temperature dependence too weak to explain the decrease of lifetimes and intensities. Moreover, experimental results are found to be the same at lower ($\approx 0.05\%$) Cr^{3+} concentrations. Therefore, this strong thermal quenching of the emission is most likely due to the dominance of multiphonon emission processes.

In this situation the experimental transition rate can be written as

$$\tau_{\text{exp}}^{-1} = \tau_R^{-1} + W_{NR} \; , \tag{5}$$

where τ_{exp} is the measured lifetime and τ_R represents the radiative lifetime, which is related to the electric dipole oscillator strength f_{em} by Eq. (2). From the measured values of the oscillator strengths at different temperatures we find a low increase of τ_R^{-1} with temperature, which is probably due to an enhancement of vibronic processes. The τ_R^{-1} rates can be fit along the temperature range of interest to the empirical formula,[34]

$$\tau_R^{-1} = \tau_0^{-1} \exp(\alpha T) \; , \tag{6}$$

and then, the temperature dependence of W_{NR} can be calculated from Eq. (5). As we shall see, W_{NR} rapidly increases with temperature in the three hosts above 77 K at nearly the same rate as luminescence decreases in the same temperature interval.

In a recent work[18] the authors found the model proposed by Struck and Fonger[19] to be adequate for a qualitative understanding of the temperature quenching of the broad-band luminescence of Cr^{3+} in BIGaZYT fluoride glass. According to these results, we tried to fit the observed temperature dependence using the current SCC model with different force constants for the ground and excited states. In this model the nonradiative decay rate at temperature T can be written as

$$W_{NR}(T) = A_{uv} U_{p_u} \; , \tag{7}$$

where A_{uv} is an electronic factor, and U_{p_u} is given by

$$U_{p_u} = \sum (1-r_v) r_v^m U_{p_u,m}^2 \; . \tag{8}$$

For parabolic energy potentials, $U_{p_u,m}^2$ are the "Franck-Condon factors" (FC) given by the Manneback recursion formula[19] and $(1-r_v)r_v^m$ are the initial v-state thermal weights, where r_v is the Boltzmann factor $\exp(-\hbar\omega_v/k_B T)$ for the initial-state phonon energy $\hbar\omega_v$. For the nonradiative transition, the v_m and u_n states are nearly resonant, satisfying the nonradiative energy balance $U_0 = p_u \hbar\omega_u$, where p_u is the number of phonons generated in the transition, and $\hbar\omega_u$ is the average phonon energy for the u level. The average m through which the nonradiative transition occurs is given by

$$\langle m \rangle_p = \sum m (1-r_v) r_v^m U_{p_u,m}^2 \; . \tag{9}$$

TABLE III. Parameters of the SCC model with different force constants for the three doped glasses.

Glass Θ	ZBL 42.89	ZBLA 42.8	ZBLAN 43.02
S_u	3.47	3.99	2.87
$\hbar\omega_u$ (cm^{-1})	563.7	546.34	612.35
S_v	2.99	3.42	2.49
$\hbar\omega_v$ (cm^{-1})	486.42	468.48	533.23
a_{uv}	3.59	3.85	3.27
U_0 (cm^{-1})	12 968	13 212	12 855
E_A (cm^{-1})	7978	7343	8896

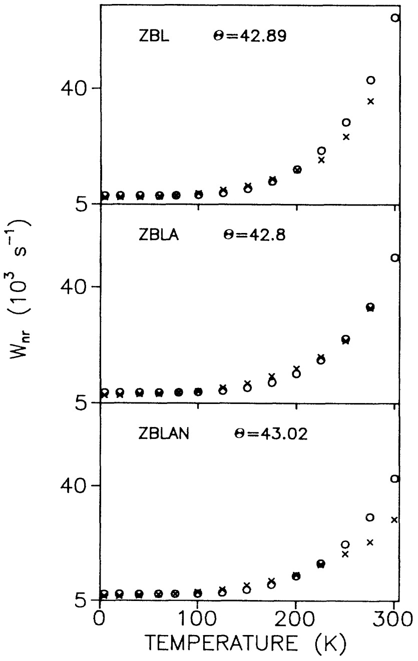

FIG. 8. Temperature dependence of measured W_{NR} (×) and the predicted quenching (○) assuming a different force constant in the ground and excited states for a Manneback angle $\Theta = 42.89$ (ZBL), 42.8 (ZBLA), and 43.02 (ZBLAN).

TABLE IV. Calculations of W_{NR} and $\langle m \rangle_p$ at four temperatures for a Manneback angle $\Theta = 42.89$ for ZBL:Cr^{3+}.

		$A_{uv}(1-r_v)r_v^m U^2_{24+m,m}$			
m	$U^2_{24+m,m}$	0 K	77 K	150 K	300 K
0	9.489×10^{-10}	9.489×10^{3}	9.488×10^{3}	9.400×10^{3}	8.568×10^{3}
1	2.055×10^{-8}		2.319×10	1.916×10^{3}	1.800×10^{4}
2	2.064×10^{-7}		2.628×10^{-2}	1.811×10^{2}	1.754×10^{4}
3	1.343×10^{-6}		1.930×10^{-5}	1.109×10	1.107×10^{4}
4	6.499×10^{-6}		1.054×10^{-8}	5.049×10^{-1}	5.197×10^{3}
5	2.522×10^{-5}		4.616×10^{-12}	1.844×10^{-2}	1.957×10^{3}
6	8.218×10^{-5}		1.698×10^{-15}	5.655×10^{-4}	6.185×10^{2}
7	2.380×10^{-4}		5.548×10^{-19}	1.541×10^{-5}	1.738×10^{2}
8	6.227×10^{-4}		1.638×10^{-22}	3.795×10^{-7}	4.410×10
9	1.491×10^{-3}		4.427×10^{-26}	8.551×10^{-9}	1.024×10
10	1.946×10^{-3}		6.520×10^{-30}	1.050×10^{-10}	1.297
	$W_{NR} = A_{uv} U_{p_u}$	9.489×10^{3}	9.511×10^{3}	1.151×10^{4}	6.318×10^{4}
	$\langle m \rangle_{24}$	0	0.002	0.201	1.935
	Crossover energy to $m \approx 17$				

In this model the Manneback angle is defined by $\tan^2\Theta = \omega_v / \omega_u$, where ω_v and ω_u are the vibrational frequencies for the excited v and ground u states ($\Theta = 45$ for linear coupling).

Table III shows the parameters values of the model for the three matrices with $\Theta = 42.89$ (ZBL), 42.8 (ZBLA), and 43.02 (ZBLAN). Figure 8 shows the measured temperature dependence of W_{NR}, and the predicted quenching from Eq. (7), taking the parameters from Table III and an electronic factor $A_{uv} = 10^{13}$ s^{-1}. After scaling W_{NR} values for comparison, a good qualitative agreement for the temperature dependence of W_{NR} can be seen. The higher value of the Manneback angle for ZBLAN:Cr^{3+} is in agreement with the lower values for nonradiative rates at high temperatures and for the FC offset a_{uv}.[35]

Tables IV–VI show the breakdown of the nonradiative rates for the ${}^4T_2(v) \rightarrow {}^4A_2(u)$ nonradiative transitions. This calculation shows the variation of the parameters with the matrix composition. In all cases the mean vibrational level at which the nonradiative transition occurs is closer to the v parabola minimum than to the v,u crossover. The mean level is 1.935 (ZBL), 2.197 (ZBLA), and 1.509 (ZBLAN) at 300 K, whereas the crossover is at $m = 17$ (ZBL), $m = 16$ (ZBLA), and $m = 17$ (ZBLAN).

Figure 9 shows, as an example, a configuration coordinate diagram for ZBLA:Cr^{3+}, using the parameters obtained for linear coupling, and for different force constants with $\Theta = 42.8$. The solid lines correspond to the potential energy wells of the electronic ground (u), and excited (v) states for $\Theta = 42.8$, whereas symbols correspond to linear coupling. As we can see, the curve crossing energy E_A decreases from 16 158 cm^{-1} to 7343 cm^{-1} as Θ decreases from 45 to 42.8 giving a lower value for the electronic coupling.

Figure 10 shows the temperature dependence of the quantum efficiency (QE) for the three samples calculated

TABLE V. Calculations of W_{NR} and $\langle m \rangle_p$ at four temperatures for a Manneback angle $\Theta = 42.8$ for ZBLA:Cr^{3+}.

		$A_{uv}(1-r_v)r_v^m U^2_{25+m,m}$			
m	$U^2_{25+m,m}$	0 K	77 K	150 K	300 K
0	5.321×10^{-10}	5.321×10^{3}	5.320×10^{3}	5.262×10^{3}	4.758×10^{3}
1	1.208×10^{-8}		1.906×10	1.335×10^{3}	1.142×10^{4}
2	1.273×10^{-7}		3.169×10^{-2}	1.573×10^{2}	1.273×10^{4}
3	8.677×10^{-7}		3.409×10^{-5}	1.198×10	9.170×10^{3}
4	4.391×10^{-6}		2.722×10^{-8}	6.778×10^{-1}	4.906×10^{3}
5	1.777×10^{-5}		1.738×10^{-11}	3.066×10^{-2}	2.099×10^{3}
6	6.022×10^{-5}		9.296×10^{-15}	1.162×10^{-3}	7.521×10^{2}
7	1.766×10^{-4}		4.302×10^{-18}	3.808×10^{-5}	2.332×10^{2}
8	5.022×10^{-4}		1.930×10^{-21}	1.210×10^{-6}	7.011×10
9	1.232×10^{-3}		7.473×10^{-25}	3.319×10^{-8}	1.818×10
10	2.218×10^{-3}		2.123×10^{-28}	6.679×10^{-10}	3.461
	$W_{NR} = A_{uv} U_p$	5.321×10^{3}	5.339×10^{3}	6.767×10^{3}	4.616×10^{4}
	$\langle m \rangle_{25}$	0	0.004	0.250	2.197
	Crossover energy to $m \approx 16$				

TABLE VI. Calculations of W_{NR} and $\langle m \rangle_p$ at four temperatures for a Manneback angle $\Theta = 43.02$ for ZBLAN:Cr^{3+}.

m	$U^2_{21+m,m}$		$A_{uv}(1-r_v)r_v^m U^2_{21+m,m}$		
		0 K	77 K	150 K	300 K
0	1.049×10^{-9}	1.049×10^{4}	1.049×10^{4}	1.043×10^{4}	9.677×10^{3}
1	2.199×10^{-8}		1.035×10	1.313×10^{3}	1.572×10^{4}
2	2.130×10^{-7}		4.717×10^{-3}	7.638×10	1.180×10^{4}
3	1.339×10^{-6}		1.395×10^{-6}	2.884	5.750×10^{3}
4	6.280×10^{-6}		3.080×10^{-10}	8.125×10^{-2}	2.090×10^{3}
5	2.369×10^{-5}		5.467×10^{-14}	1.841×10^{-3}	6.111×10^{2}
6	7.527×10^{-5}		8.174×10^{-18}	3.513×10^{-5}	1.505×10^{2}
7	2.217×10^{-4}		1.133×10^{-21}	6.216×10^{-7}	3.435×10
8	5.257×10^{-4}		1.264×10^{-25}	8.853×10^{-9}	6.312
9	1.265×10^{-3}		1.432×10^{-29}	1.280×10^{-10}	1.177
10	1.328×10^{-3}		7.072×10^{-34}	8.068×10^{-13}	9.578×10^{-2}
	$W_{NR} = A_{uv} U_p$	1.049×10^{4}	1.050×10^{4}	1.182×10^{4}	4.584×10^{4}
	$\langle m \rangle_{21}$	0	0.001	0.125	1.509
	Crossover energy to $m \approx 17$				

by the expression $\eta = \tau_{\exp}/\tau_R$. As can be seen, the QE rapidly decreases as temperature increases above 150 K, which is a typical behavior of Cr^{3+} in glassy systems,[15] indicating the existence of Cr^{3+} in sites that have significant nonradiative relaxation even at low temperatures. This low-temperature QE could be related to the so-called bottom crossover.[19]

It is worthwhile noticing that the highest QE values correspond to the ZBLAN matrix according to the parameter values obtained for this sample from the Struck-Fonger model: i.e., the highest value for the Manneback angle, the lowest value for the FC offset a_{uv},[35] and the highest value for the crossover energy E_A (see Table III). Assuming that the excited and ground-state configurations of Cr^{3+} ions in these glasses differ from each other, this variation is more pronounced in ZBLA and ZBL glasses giving an enhancement of nonradiative transition rates and therefore a lower value for QE. From the point of view of chemical composition, this behavior may be connected with a more rigid and closed structure in the ZBLAN glass, which could restrict the nonradiative transitions of chromium ions. With the addition of NaF, the Ba^{2+} network modifier is partially replaced by Na^{+},[36] thus decreasing the number of nonbridged F^{-} ions as ionic conductivity measurements show.[37] On the other hand, Raman reflectance data[38] suggest that the addition of aluminum suppresses the strong local structure of the base glass and introduces greater disorder, which could increase the probability of nonradiative transitions.

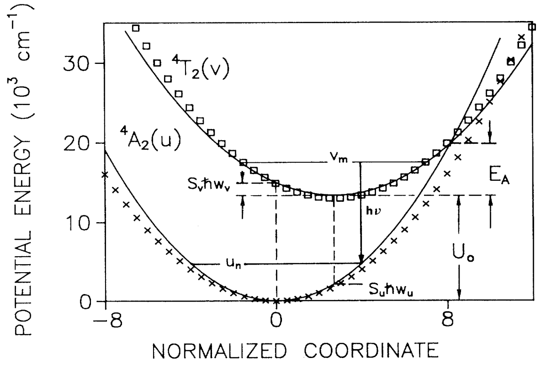

FIG. 9. Single configurational coordinate diagram for ZBLA:Cr^{3+} based on the parameters obtained for linear coupling ($\Theta = 45°$), and for a Manneback angle of 42.8. Solid lines correspond to the potential energy wells of the electronic ground (u) and excited (v) states for $\Theta = 42.8$, and symbols correspond to linear coupling. U_0 represents the electronic gap, S is the Huang-Rhys factor, u_n and v_m are the initial and final vibrational wave functions, $S_u\hbar\omega_u$ and $S_v\hbar\omega_v$ are the relaxation energies after emission and absorption, respectively, and E_A is the curve crossing energy. Linear coupling corresponds to $\hbar\omega_u = \hbar\omega_v = \hbar\omega_0$ and $S_u = S_v = S$.

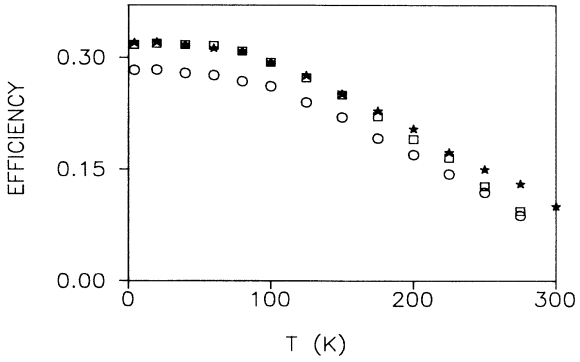

FIG. 10. Quantum efficiency as a function of temperature for Cr^{3+} in the matrices ZBL (□), ZBLA (○), and ZBLAN (★).

We made no effort to calculate absolute values of W_{NR}, as current theories do not seem adequate to this task. Nor did we attempt to analyze the data by using models of nonradiative decays, which emphasize anharmonic effects.

C. Site-dependent effects on fluorescence

As we mentioned before (Sec. III), the mean features of the absorption and emission spectra of Cr^{3+} in ZBL-type glasses can be broadly interpreted in terms of a crystal-field diagram. Because of the structural disorder inherent to a glass, we might expect a large continuous range of slightly distorted octahedral sites available to Cr^{3+} ions. Due to the spread of Dq/B values from site to site, a broad range of energy levels and radiative and nonradiative transition probabilities are available for a narrow laser exciting wavelength. As an example of this, Fig. 11 shows the LNT fluorescence of ZBLA following excitations into the $^4T_1$ band. A narrowing (≈ 52 cm^{-1}), and a red shift (≈ 237 cm^{-1}) of the spectra can be observed when excitation wavelength increases from 476 to 514 nm. Figure 12 shows an extended Tanabe-Sugano diagram taking into account the spread of the Dq/B values for the different Cr^{3+} sites. When pumping with a 476-nm wavelength, a large group of sites is raised to the $^4T_1$ state, nearly the same number as were obtained by exciting with the 633-nm line into the $^4T_2$ band. On the other hand, using the 514-nm line on the long-wavelength edge of the $^4T_1$ band, we selectively excite a lower number of sites with smaller Dq values. After a rapid electronic relaxation by nonradiative transitions to the lower $^4T_2$ level, these sites will give the narrowed fluorescence spectrum observed in Fig. 11.

The above results were also found for Cr^{3+} ions in other glass matrices[39] and for Mo^{3+} in phosphate glass.[31] Nevertheless, the experimental results on fluorescence lifetimes and time-resolved spectra, shown in the preceding sections, point to the existence of two main site distributions for Cr^{3+} ions in ZBL-type glasses. The structural order in the host matrix of these glasses seems to be dominated by well-defined structural units consisting of Zr with F.[40] Recent ^{19}F NMR studies in ZBL glass[41] have revealed the presence of three discrete fluoride-ion sites in the glass structure. These data reinforce the assumption of one site having a fluorine ion tightly bound to one or more Zr^{4+} cations and the other two sites having the fluorine ions situated in environments influenced by Ba^{2+} and/or La^{3+} cations and therefore weakly bound. Due to the importance of bonding requirements, we can expect two nearly octahedral site distributions for Cr^{3+} ions in these matrices, depending on the local environment established during the formation of the glass.

As we have seen before, for a given excitation wavelength a large group of sites with slightly different Dq/B values can be raised to the $^4T_2$ excited state. After rapid nonradiative relaxation to the lower end of the $^4T_2$ band a radiative Stokes-shifted emission to the $^4A_2$ ground state will take place with wavelengths and decay times that are characteristic of the site distribution. Figure 4 (Sec. III B) showed the average lifetimes within the $^4T_2 \rightarrow {}^4A_2$ emission band after excitation with the 655-nm line. It is worthwhile noticing the two steps shown by the three samples as the emission wavelength increases from the high- to the low-energy side of the emission band. If only one kind of site distribution were to be present, a monotonic decrease of lifetimes with increasing emission wavelength should be expected (ions having larger Dq values will have lower nonradiative transition

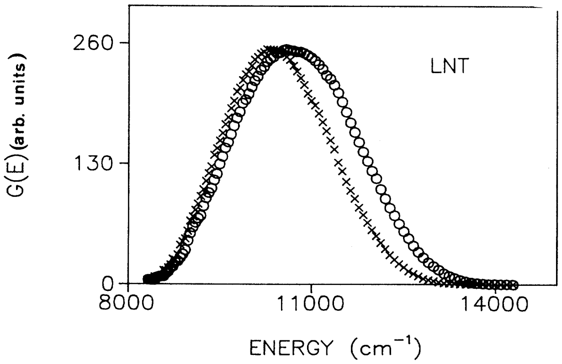

FIG. 11. LNT steady-state (SS) emission spectra of ZBLA:Cr^{3+} obtained by exciting at the $^4T_1 \leftarrow {}^4A_2$ absorption band with the 476-nm (○) and 514-nm (×) lines of an Argon laser. The corrected spectra have been normalized to have the same peak intensity.

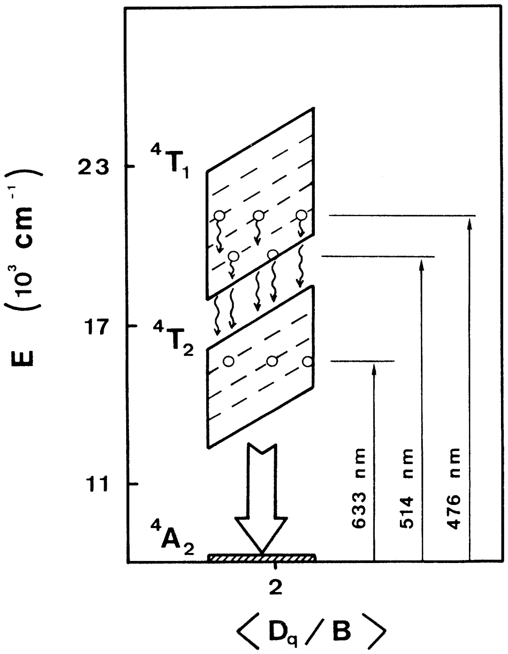

FIG. 12. Extended Tanabe-Sugano diagram in fluorozirconate glasses. The straight lines represent excitations, the broad arrow emissions to the ground state, and the undulating lines nonradiative relaxations.

probabilities and longer lifetimes). These results are consistent with a model of two or more subsets of Cr^{3+} ions with slightly different spectral dependences. In addition to this two-step behavior of the average lifetimes, the biexponential character shown by the shape of lifetime curves under laser excitation also reinforces this hypothesis. As we shall see below, energy transfer or cross relaxation between Cr^{3+} ions in spectrally different sites can be disregarded as shown by time-resolved fluorescence.

The influence of different sites on the time dependence of emission spectra may help to clarify our understanding of the Cr^{3+} site distributions. At short time delays (1 μs) the TRS emission spectra do not show significant differences from the SS spectra, and the fluorescence is characteristic of the whole distribution of ions. When time increases, the ions with the shorter lifetimes have decayed and make no contribution to the delayed fluorescence. As a consequence a blue shift and a monotonic narrowing should appear.[31] In spite of this, Fig. 6 showed that the blue-shift and half-width narrowing display an abrupt change in the time interval between 1 and 50 μs. This interval of time roughly covers the short-lived component of the experimental decays. If energy transfer or cross-relaxation between Cr^{3+} ions were present, energy would migrate towards the lower energy sites giving a red shift instead of the blue one observed.

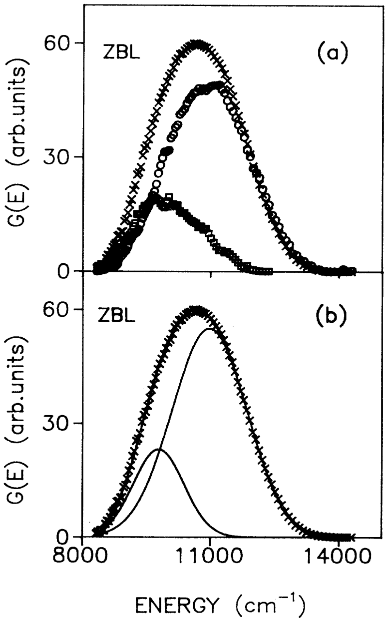

FIG. 13. (a) Comparison of scaled time-resolved emission spectrum (○) of $^4T_2\rightarrow{}^4A_2$ transition in ZBL:Cr^{3+} at a time delay of 300 μs (excited at 655 nm), and steady-state (SS) emission spectrum (×) (excited at 633 nm). The difference between both spectra is represented by (□). (b) SS emission intensity of $^4T_2\rightarrow{}^4A_2$ transition. Experiment is shown by ×; fit is to a double Gaussian function (solid line). Measurements were performed at 77 K.

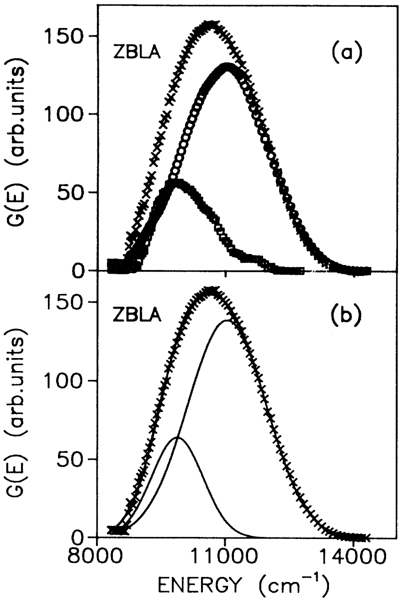

FIG. 14. (a) Comparison of scaled time-resolved emission spectrum (○) of $^4T_2\rightarrow{}^4A_2$ transition in ZBLA:Cr^{3+} at a time delay of 300 μs (excited at 655 nm) and steady-state (SS) emission spectrum (×) (excited at 633 nm). The difference between both spectra is represented by (□). (b) SS emission intensity of $^4T_2\rightarrow{}^4A_2$ transition. Experiment is shown by ×; fit is to a double Gaussian function (solid line). Measurements were performed at 77 K.

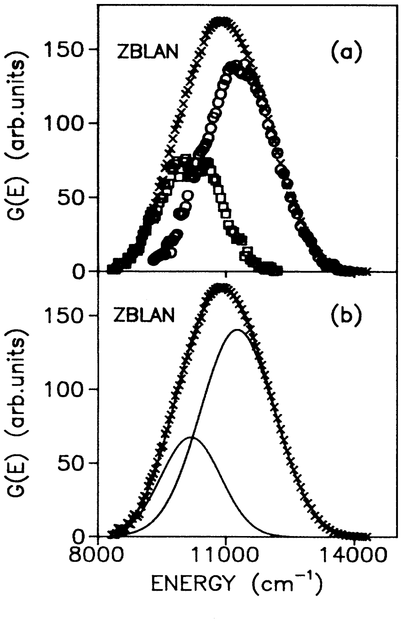

FIG. 15. (a) Comparison of scaled time-resolved emission spectrum (○) of $^4T_2\rightarrow{}^4A_2$ transition in ZBLAN:Cr^{3+} at a time delay of 300 μs (excited at 655 nm) and steady-state (SS) emission spectrum (×) (excited at 633 nm). The difference between both spectra is represented by (□). (b) SS emission intensity of $^4T_2\rightarrow{}^4A_2$ transition. Experiment is shown by ×; fit is to a double Gaussian function (solid line). Measurements were performed at 77 K.

This behavior was found in the three samples studied.

In order to give a qualitative idea about the existence of a distribution of low field sites characterized by short relaxation times (≈ 50 μs) we compared the LNT time-resolved spectra of the three samples, obtained with a time delay of 300 μs, with the SS spectra. On the top of Figs. 13, 14, and 15 we can see the difference between both spectra scaled at the high-energy wing of the emission band. As can be observed these differences are nearly Gaussian and red shifted, corresponding to the luminescence loss attributed to the low-energy site distribution of each sample. Bearing this in mind, we tried to fit the SS spectra to two Gaussian functions and obtained an excellent fit by the standard Marquard procedure as shown at the bottom of Figs. 13, 14, and 15. It is interesting to notice the good qualitative agreement between the low-energy Gaussian curves in Figs. 13(b)–15(b) and the scaled differences in Figs. 13(a)–15(a), which can be interpreted as a further evidence of two distinguishable distributions of Cr^{3+} sites in these glass matrices.

V. CONCLUSIONS

(i) The optical properties of Cr^{3+} ions in ZBL-type glasses have been studied. From steady-state optical absorption and luminescence measurements we conclude that Cr^{3+} is incorporated, on the average, in octahedrally coordinated sites. The spectroscopic data in Table I show that Cr^{3+} ions in these glasses have a weak crystal field and, therefore, the emission is characterized by a broad and structureless ${}^4T_2 \rightarrow {}^4A_2$ band.

(ii) The QMSCC model with different constant forces gives a good qualitative agreement with the experimental temperature dependence of W_{NR} for the three glasses studied.

(iii) Quantum efficiencies at room temperature are low in accordance with the strong thermal quenching of luminescence.

(iv) The influence of the glass composition on the QE values can be correlated with the parameters obtained from the QMSCC model. From the point of view of chemical composition, the differences in the QE measured values for the three glasses may be connected with changes in the available bondings between metal and fluorine (bridged and nonbridged), and to the sensitivity of the Cr^{3+} excited state to different next-neighbor environments, which can be changed by ion modifiers.

(v) The narrowing observed in the SS emission spectra when exciting wavelength increases from 476 to 514 nm, on the ${}^4T_1 \leftarrow {}^4A_2$ band, reveals the existence of a broad distribution of Cr^{3+} sites due to the spread of Dq/B values in these glasses. Moreover, the wavelength dependence shown by lifetimes along the ${}^4T_2 \rightarrow {}^4A_2$ emission band and the biexponential behavior of the decay provide evidences for the existence of two main site distributions for Cr^{3+} in these glasses.

(vi) The blue shift and narrowing of the TR emission spectra undergo an abrupt change in the time interval between 1 and 50 μs. This confirms the existence of a subset of low-field sites characterized by short relaxation times, which can be also qualitatively observed by comparing SS and long-time delayed emission spectra.

ACKNOWLEDGMENTS

This work was supported by the Comisión Interministerial de Ciencia y Tecnologia (CICYT) of the Spanish Government (Ref. No. 0188/89) and Basque Country Government (Ref. No. 0008/89).

---

[1] M. M. Broer and L. G. Cohen, J. Lightwave Tech. **LT-4**, 1509 (1986).
[2] L. Reekie, R. J. Mears, S. B. Poole, and D. N. Payne, J. Lightwave Tech. **LT-4**, 956 (1986).
[3] R. S. Quimby, M. G. Drexhage, and M. J. Suscavage, Electron. Lett. **23**, 32 (1987).
[4] D. C. Yeh, W. A. Sibley, M. Suscavage, and M. G. Drexhage, J. Appl. Phys. **62**, 266 (1987).
[5] M. G. Drexhage, in *Treatise on Materials Science and Technology*, edited by M. Tomozawa and R. H. Doremus (Academic, New York, 1985), Vol. 26, pp. 151–243.
[6] K. Tanimura, M. D. Shinn, W. A. Sibley, M. G. Drexhage, and R. N. Brown, Phys. Rev. B **30**, 2429 (1984).
[7] J. L. Adam and W. A. Sibley, J. Non-Cryst. Solids **76**, 267 (1985).
[8] M. Eyal, E. Greenberg, R. Reisfeld, and N. Spector, Chem. Phys. Lett. **117**, 108 (1985).
[9] R. Reisfeld, M. Eyal, E. Greenberg, and C. K. Jorgensen, Chem. Phys. Lett. **118**, 25 (1985).
[10] B. Moine, A. Brenier, and C. Pedrini, IEEE J. Quantum Electron. **QE-25**, 88 (1989).
[11] Y. Suzuki, W. A. Sibley, O. H. El Bayoumi, T. M. Roberts, and B. Bendow, Phys. Rev. B **35**, 4472 (1987).
[12] E. Snow, J. A. Freitas, Jr., and U. Strom, Phys. Rev. B **37**, 10 332 (1988).
[13] P. T. Kenyon, L. J. Andrews, B. C. McCollum, and A. Lempicki, IEEE J. Quantum Electron. **QE-18**, 1189 (1982).
[14] R. Reisfeld, Mater. Sci. Eng. **71**, 375 (1985).
[15] L. J. Andrews, A. Lempicki, and B. C. McCollum, J. Chem. Phys. **74**, 5526 (1981).
[16] S. A. Payne, L. L. Chase, and W. F. Krupke, Chem. Phys. **86**, 3455 (1987).
[17] G. F. Imbusch, T. J. Glynn, and G. P. Morgan, J. Lumin. **45**, 63 (1990).
[18] M. A. Illarramendi, J. Fernández, R. Balda, J. Lucas, and J. L. Adam, J. Lumin. **47**, 207 (1991).
[19] C. W. Struck and W. H. Fonger, J. Lumin. **10**, 1 (1975).
[20] R. Balda, M. A. Illarramendi, J. Fernández, and J. Lucas, J. Lumin. **45**, 87 (1990).
[21] A. Lecoq and M. Poulain, Verres Réfract. **34**, 333 (1980).
[22] R. E. Tischer, J. Chem. Phys. **48**, 4291 (1968).
[23] L. L. Lohr, J. Chem. Phys. **50**, 4596 (1969).
[24] G. O. Karapetyan, S. G. Lunter, and D. M. Yudin, Opt. Spectrosc. **14**, 370 (1963).

[25]H. L. Schlafer, H. Gausmann, and H. Witzke, J. Chem. Phys. **46**, 1423 (1967).

[26]J. Fano, Phys. Rev. **124**, 1866 (1961).

[27]A. Lempicki, L. J. Andrews, S. Nettle, B. C. McCollum, and E. I. Salomon, Phys. Rev. Lett. **44**, 1234 (1980).

[28]S. Sugano, Y. Tanabe, and H. Kamimura, *Multiplets of Transition-Metal Ions in Crystals* (Academic, New York, 1970).

[29]B. Di Bartolo, *Optical Interactions in Solids* (Wiley, New York, 1968).

[30]D. E. McCumber, Phys. Rev. **136**, A954 (1964).

[31]M. J. Weber, S. A. Brawer, and A. J. DeGroot, Phys. Rev. B **23**, 11 (1981).

[32]A. J. Wojtowicz, M. Kazmierczak, A. Lempicki, and R. H. Bartram, J. Opt. Soc. Am. B **6**, 1106 (1989).

[33]C. W. Struck and W. H. Fonger, J. Lumin. **18/19**, 101 (1979).

[34]L. J. Andrews, A. Lempicki, B. C. McCollum, C. J. Giunta, R. H. Bartram, and J. F. Dolan, Phys. Rev. B **34**, 2735 (1986).

[35]G. Blasse, in *Radiationless Processes,* edited by B. DiBartolo (Plenum, New York, 1980), p. 287.

[36]R. Gatzke, Ceram. Bull. **68**, 1946 (1989).

[37]J. M. Reau, H. Kahnt, and M. Poulain, J. Non-Cryst. Solids **119**, 347 (1990).

[38]B. Bendow *et al.*, J. Am. Ceram. Soc. **66**, C-64 (1983).

[39]C. Fuxi and L. Huimin, J. Non-Cryst. Solids **80**, 20 (1986).

[40]B. Bendow *et al.*, J. Am. Ceram. Soc. **68**, C-92 (1985).

[41]D. R. MacFarlane, J. O. Browne, T. J. Bastow, and F. W. West, J. Non-Cryst. Solids **108**, 289 (1989).